



A Pseudorabies Virus Serine/Threonine Kinase, US3, Promotes Retrograde Transport in Axons via Akt/mTORC1

Andrew D. Esteves,^a Orkide O. Koyuncu,^{a*} Lynn W. Enquist^a

^aDepartment of Molecular Biology, Princeton University, Princeton, New Jersey, USA

ABSTRACT Infection of peripheral axons by alpha herpesviruses (AHVs) is a critical stage in establishing a lifelong infection in the host. Upon entering the cytoplasm of axons, AHV nucleocapsids and associated inner-tegment proteins must engage the cellular retrograde transport machinery to promote the long-distance movement of virion components to the nucleus. The current model outlining this process is incomplete, and further investigation is required to discover all viral and cellular determinants involved as well as the temporality of the events. Using a modified tri-chamber system, we have discovered a novel role of the pseudorabies virus (PRV) serine/threonine kinase US3 in promoting efficient retrograde transport of nucleocapsids. We discovered that transporting nucleocapsids move at similar velocities in both the presence and absence of a functional US3 kinase; however, fewer nucleocapsids are moving when US3 is absent, and they move for shorter periods of time before stopping, suggesting that US3 is required for efficient nucleocapsid engagement with the retrograde transport machinery. This led to fewer nucleocapsids reaching the cell bodies to produce a productive infection 12 h later. Furthermore, US3 was responsible for the induction of local translation in axons as early as 1 h postinfection (hpi) through the stimulation of a phosphatidylinositol 3-kinase (PI3K)/Akt-mTORC1 pathway. These data describe a novel role for US3 in the induction of local translation in axons during AHV infection, a critical step in transport of nucleocapsids to the cell body.

IMPORTANCE Neurons are highly polarized cells with axons that can reach centimeters in length. Communication between axons at the periphery and the distant cell body is a relatively slow process involving the active transport of chemical messengers. There is a need for axons to respond rapidly to extracellular stimuli. Translation of repressed mRNAs present within the axon occurs to enable rapid, localized responses independently of the cell body. AHVs have evolved a way to hijack local translation in the axons to promote their transport to the nucleus. We have determined the cellular mechanism and viral components involved in the induction of axonal translation. The US3 serine/threonine kinase of PRV activates Akt-mTORC1 signaling pathways early during infection to promote axonal translation. When US3 is not present, the number of moving nucleocapsids and their processivity are reduced, suggesting that US3 activity is required for efficient engagement of nucleocapsids with the retrograde transport machinery.

KEYWORDS Akt, PRV, axon, retrograde transport, US3, mTORC1, translation, viral entry, kinase, intracellular transport, pseudorabies virus

Members of the alpha herpesvirus (AHV) subfamily, including the human pathogens herpes simplex virus 1 and 2 (HSV-1 and HSV-2), as well as the animal pathogen, pseudorabies virus (PRV), are pantropic viruses capable of infecting the peripheral nervous system (PNS) and central nervous system (CNS) of their hosts. Infection of the highly polarized PNS at axon terminals occurs after infection of the

Editor Felicia Goodrum, University of Arizona

Copyright © 2022 Esteves et al. This is an open-access article distributed under the terms of the [Creative Commons Attribution 4.0 International license](https://creativecommons.org/licenses/by/4.0/).

Address correspondence to Andrew D. Esteves, aesteves@princeton.edu, or Lynn W. Enquist, lenquist@princeton.edu.

*Present address: Orkide O. Koyuncu, Department of Microbiology and Molecular Genetics, School of Medicine, University of California, Irvine, Irvine, California, USA.

The authors declare no conflict of interest.

Received 11 October 2021

Accepted 17 December 2021

Accepted manuscript posted online

5 January 2022

Published 9 March 2022

epithelial layer. Once in the axonal cytoplasm, nucleocapsids undergo efficient retrograde transport to the nucleus, where the viral DNA is transcribed and either a productive or a lifelong latent infection is established. In natural hosts, AHVs tend to establish a latent infection. Reactivation from latency results in the anterograde transport of progeny virion particles in the axon to reinfect the epithelial layer that promotes spread to new hosts. In rare events, progeny virion particles can spread in the opposite direction and transsynaptically invade the CNS, often leading to death of the organism. In nonnatural hosts, a productive infection followed by invasion of the CNS and death are the most common (1).

The recruitment of the retrograde transport machinery to mediate the active transport of virion particles is facilitated by the viral nucleocapsid and inner-tegment proteins (UL36, UL37, and US3) (2, 3). This process, while dispensable in nonpolarized cells, is essential for neuronal infection via axons due to the large distance between the axon terminal and the cell body (3–5). Despite this, the viral and cellular factors involved and the temporality of the events are not well understood. Following fusion of the viral and cellular membranes, a breach in the actin cytoskeleton is created through the activation of cofilin by the US3 protein (6). The microtubule plus-tip proteins EB-1 and CLIP170 also have been shown to aid in this process during HSV-1 infection (7). The UL36 inner-tegment protein then interacts with dynactin, to recruit the nucleocapsid complex to dynein, the retrograde-directed motor protein (8, 9). UL37, even though it has not been shown to interact with dynein, is capable of modulating its activity (4). We have previously shown that upon infection of axons with PRV, translation of a subset of axonally localized mRNA occurs, producing a subset of proteins related to intracellular transport and cytoskeletal remodeling (10). Among these is the dynein regulator Lis1. Local translation in axons was shown to be essential for the efficient transport of virion components through the axon; however, the mechanism that regulates this is unknown.

Translation of cellular mRNA is a tightly regulated process, with the initiation stage being the most rate limiting. The phosphatidylinositol 3-kinase (PI3K)/Akt-mTORC1 signaling pathway is the canonical route by which translation initiation occurs in eukaryotic cells (11). AHVs have been demonstrated to manipulate this signaling pathway to support infection and replication. HSV-2 infection induces Akt phosphorylation upon binding of gB, on the virion envelope, to $\alpha_3\beta_3$ integrins, leading to release of intracellular calcium stores to promote entry of nucleocapsids into the cell (12, 13). In HSV-1-infected cells, Akt phosphorylation increased at early times after infection but was suppressed after virus replication (14). At these later stages of infection, activation of mTORC1 was induced by the phosphorylation of Akt substrates in an Akt-independent manner. This work demonstrated that a viral kinase could act as an Akt surrogate to bypass cellular signal pathway control mechanisms to promote constitutive viral replication (15). In varicella-zoster virus (VZV)-infected cells Akt phosphorylation is increased and required for efficient replication (16–18). PRV infection induces Akt phosphorylation to mediate antiapoptosis effects on infected cells (19). Despite these findings in non-neuronal cells, it is not known if AHV infection of axons induces Akt signaling pathways. In this study, we investigated whether PRV infection stimulates the Akt-mTORC1 signaling pathway to induce local translation in axons.

US3 is a multifunctional, virus-encoded serine/threonine kinase present in the inner-tegment layer of the virion and one of only two protein kinases conserved by all AHVs (20). Although US3 has been shown to be dispensable for virus replication in cell culture, it is vital for viral fitness *in vivo* (21–26). Some of the most notable functions of US3 include the inhibition of apoptosis in infected cells through the activation of Akt and NF- κ B signaling pathways, promotion of nuclear egress of newly made nucleocapsids, and disassembly of actin stress fibers by cofilin activation (27–29). Due to its serine/threonine kinase function, its known interactions with Akt, and its presence in the tegument layer, and thus its direct delivery to the cytoplasm, we hypothesized

that US3 stimulates Akt-mTORC1 signaling pathways in axons early after infection, to induce local translation.

In this study, we established a novel role for PRV US3 in the induction of translation in axons via a PI3K/Akt-mTORC1 signaling pathway early after virion entry to promote the efficient retrograde transport of nucleocapsids to the cell body. In the absence of US3 or Akt phosphorylation, the number of transporting nucleocapsids and their processivity were significantly reduced. These events led to a reduction in the number of infected neuronal cell bodies later in infection. Together, these findings suggest a role for US3 in the continuous engagement of PRV nucleocapsids with the retrograde transport machinery. Due to the significance this stage of infection plays in AHV infection of neurons at the axon, US3 may serve as a target for drugs aiming to prevent the life-long, reactivatable infection caused by AHVs.

RESULTS

Akt is phosphorylated in axons early after PRV infection. To determine if Akt is phosphorylated in axons early after PRV infection, we cultured primary rat superior cervical ganglion (SCG) neurons *in vitro* in Campenot trichambers (Fig. 1A). This cell culture system allows the fluidic separation of neuronal cell bodies (in the S compartment) from axons (in the N compartment), enabling us to infect pure populations of axons and monitor responses independently of the cell bodies (30). N-compartment axons were infected with 10^6 PFU of a PRV-Becker recombinant expressing a monomeric red fluorescent protein (mRFP)-tagged capsid protein (VP26) termed PRV 180. Akt phosphorylation was monitored using a phospho-S⁴⁷³-Akt (p-S⁴⁷³-Akt) antibody. Phosphorylation at serine 473 is the best-known mechanism of Akt activation (31); it can be observed as early as 30 min postinfection (mpi) in axons and continues to at least 180 mpi (Fig. 1B), indicating that PRV infection does induce Akt phosphorylation in axons. Furthermore, when axons in the N compartment were pretreated with LY294002 (a potent and selective PI3K inhibitor) prior to infection, no Akt phosphorylation was observed, suggesting that PRV-induced Akt phosphorylation is PI3K dependent (Fig. 1C). When axons were pretreated with the mTORC1 inhibitor rapamycin or the translation inhibitor cycloheximide, Akt phosphorylation did occur (Fig. 1C). No change in Akt phosphorylation occurred in S-compartment cell bodies 1 h postinfection (hpi) when the N compartment was infected, demonstrating that the infection and intracellular signals do not reach the cell body in that time (Fig. 1D).

Akt phosphorylation in axons is required for efficient retrograde transport of PRV nucleocapsids. Next, we determined whether infection-induced Akt phosphorylation in axons affected the spread of PRV to the distant cell body. N compartments were treated with a green lipophilic dye, Fast-DiO, to label the membranes of all axons in the N compartment and their attached cell bodies in the S compartment such that only the cell bodies with axons extended into the N compartment were labeled. At 12 h after DiO staining, N compartments were infected with PRV 180 (Fig. 2A). At 12 hpi, infected cell bodies were visualized by the presence of red fluorescence from the mRFP-VP26 fusion protein (Fig. 2B). The presence of dual-colored cell bodies (expressing red and green fluorescence) corresponded to those that were directly infected via axons in the N compartment. The ratio of dual-colored cell bodies to total green cell bodies represents the efficiency of retrograde infection. When N-compartment axons were pretreated with Akt inhibitor VIII for 1 h prior to infection, we observed an $\sim 56.4\% \pm 14.7\%$ reduction in the number of dual-colored cell bodies compared to PRV 180 infection alone. Additionally, when axons were pretreated with LY294002, rapamycin, or cycloheximide, dual-colored cell bodies were reduced by $\sim 48\% \pm 16.2\%$, $\sim 58\% \pm 17.6\%$, and $\sim 65.7 \pm 9.5\%$, respectively. Ras/MAPK is also known to promote translation by signaling through mTORC1 (32–37); however, pretreatment of axons with the Erk1/2 inhibitor U0126 had no significant effect on retrograde infection ($\sim 8.3\% \pm 14\%$) (Fig. 2C).

Local translation of axonal mRNA after PRV infection promoted the efficient retrograde transport of nucleocapsids through the axon (10). To determine if Akt-mTORC1 is

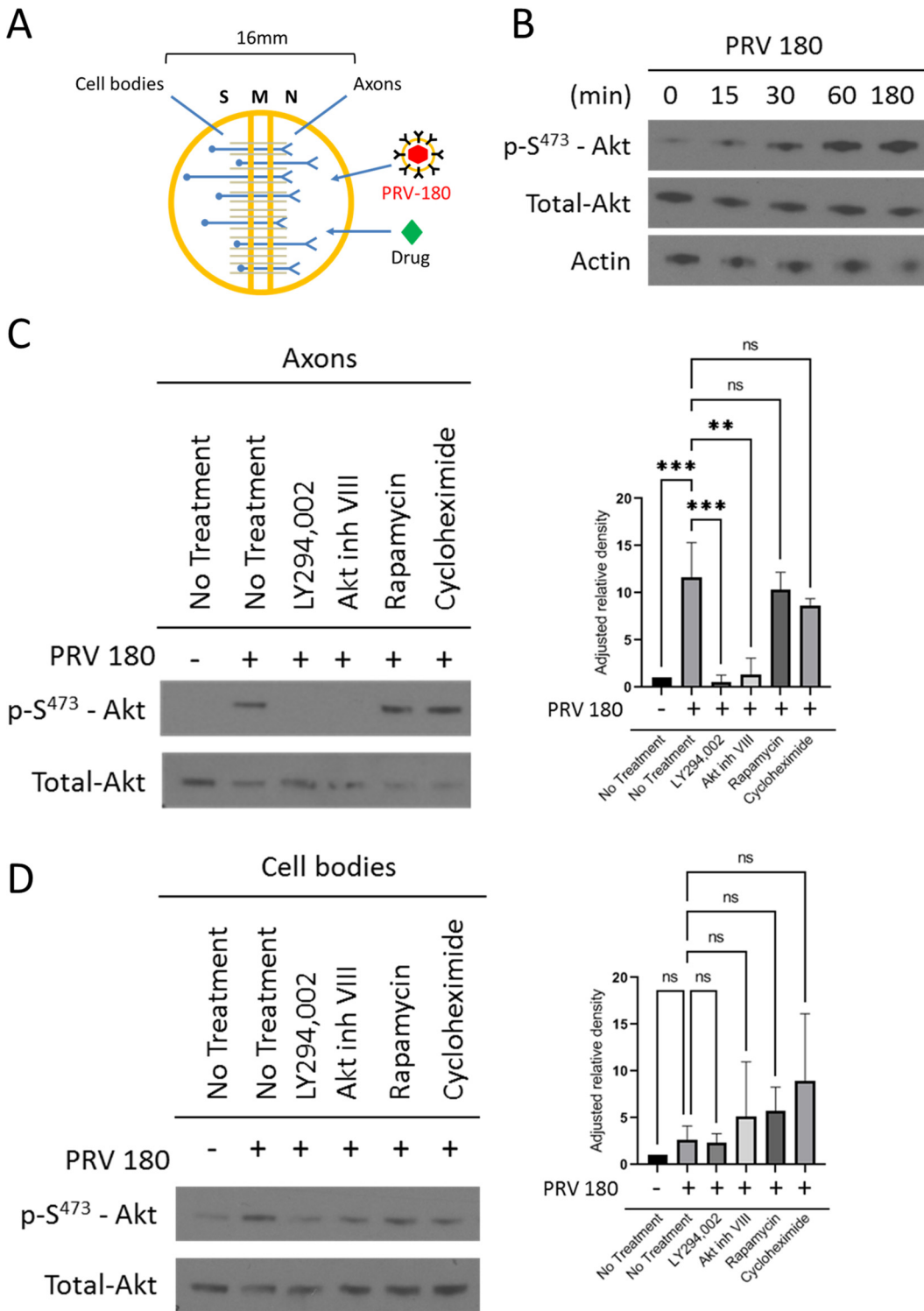


FIG 1 Akt is phosphorylated in axons during PRV infection. (A) A Campenot trichamber neuronal culture system divided into soma (S), middle (M), and neurite (N) compartments used to separate neuronal cell bodies from axons. Addition of virus or drug into the N compartment allows the study of axonal responses independent of the cell body. (B and C) Immunoblots of p-S⁴⁷³-Akt in axons infected with PRV 180 in the N compartment. (B) Infections continued for 0 min, 15 min, 30 min, 60 min, and 180 min. (C and D) N compartments were pretreated with LY294002, Akt inhibitor VIII, rapamycin, or cycloheximide prior to infection. (C) N compartments were harvested 1 hpi. (D) S compartments were harvested 1 hpi in the N compartment. (C and D) p-S⁴⁷³-Akt bands were normalized to total-Akt bands using a densitometry assay. Means and standard deviations (SD) for condition ($n = 3$) are plotted. **, $P \leq 0.01$, and ***, $P \leq 0.001$, using one-way analysis of variance (ANOVA); ns, not significant.

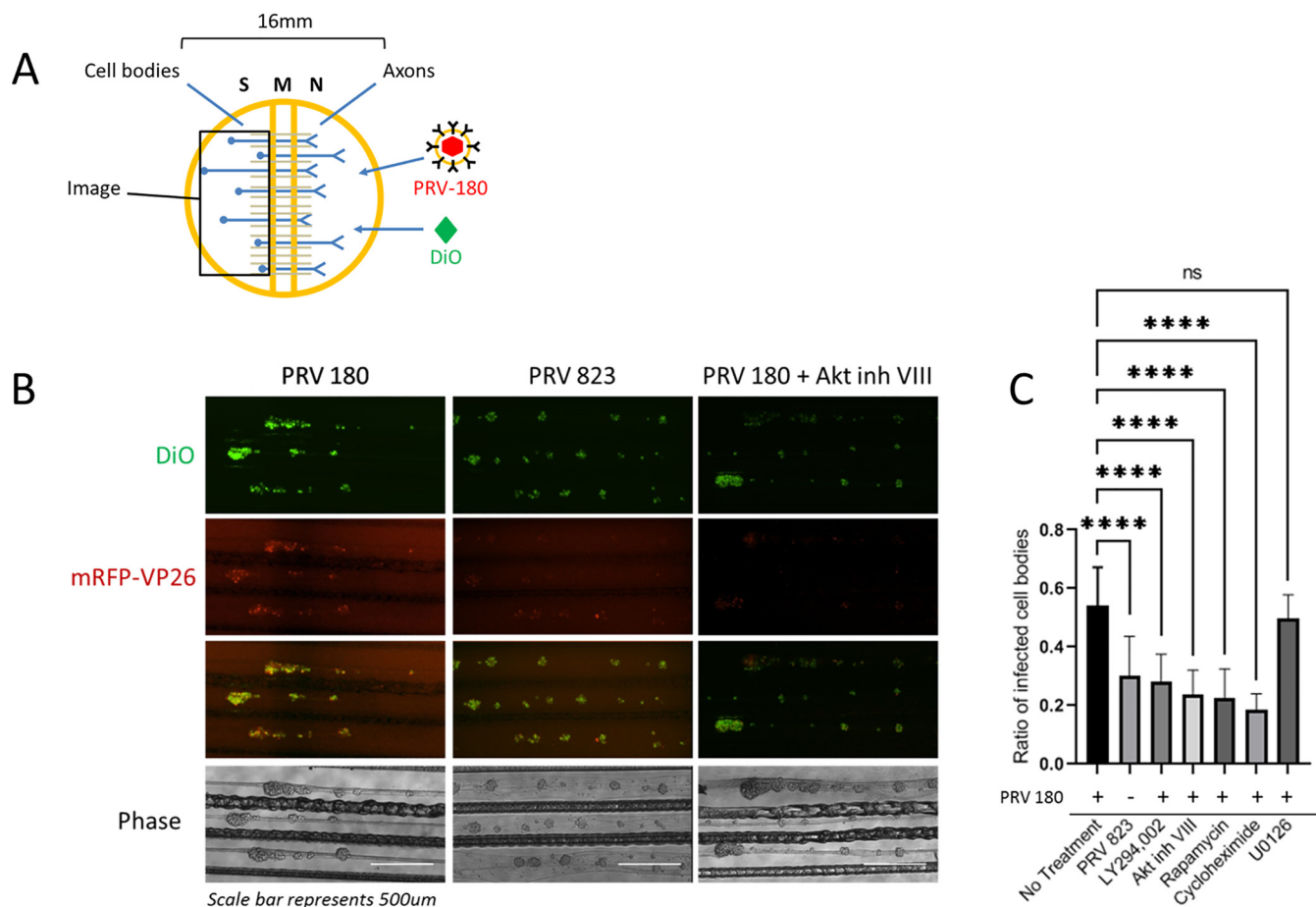


FIG 2 Disruption of Akt signaling pathways reduced PRV retrograde infection. (A) N-compartment axons were treated with FAST-DiO 12 h prior to infection. PRV 180 or PRV 823 was added to axons, and at 12 hpi, S-compartment cell bodies were tile imaged. For conditions involving inhibitor treatment, inhibitor was added to N compartments 1 h prior to infection, and at 6 hpi, unabsorbed virus inoculum and inhibitor were removed from the N compartment. (B) Tile images of neuron cell bodies in S compartments. Bar, 500 μ m. (C) Quantification of primarily infected cells. The ratio of dual-colored to total green cell bodies for each condition was calculated. Means and SD for 10 chambers for each condition are plotted. ****, $P \leq 0.0001$, using one-way ANOVA; ns, not significant.

also required for efficient transport, N-compartment axons were infected with PRV 180 and at 2 hpi, videos of fluorescent nucleocapsids trafficking through the M (middle) compartment were recorded (Fig. 3A). Maximum intensity projections and kymographs were created from the videos of moving nucleocapsids to analyze transport kinetics (Fig. 3B). Moving nucleocapsids were represented as continuous “tracks.” When N compartments were pretreated with LY294002, Akt inhibitor VIII, rapamycin, or cycloheximide, the number of moving nucleocapsids was reduced by $\sim 75.8\% \pm 24.4\%$, $\sim 76.3\% \pm 24.4\%$, $\sim 79\% \pm 22.8\%$, or $\sim 75.8\% \pm 40.8\%$, respectively, compared to PRV 180 infection alone (Fig. 3C). The net displacement of moving nucleocapsids (length of tracks) was also reduced by $\sim 50\%$ when these inhibitors were present (Fig. 3D). Nevertheless, the velocity of nucleocapsids that were moving under each condition was the same (Fig. 3E), suggesting that engagement with the transport machinery, not the transport speed, was disrupted. U0126 treatment had no significant effect on nucleocapsid transport or processivity. Taken together, these data demonstrate that Akt-mToRC1 signaling is promoted by PRV infection in axons and is required for efficient retrograde transport of nucleocapsids. It should be noted, however, that the effect of these inhibitors on transport of cellular cargos was not investigated, and it may possibly play a role in mediating transport of nucleocapsids. These effects were comparable to those observed when translation was blocked, suggesting that Akt-mToRC1 activation acts early after PRV infection to promote translation in axons.

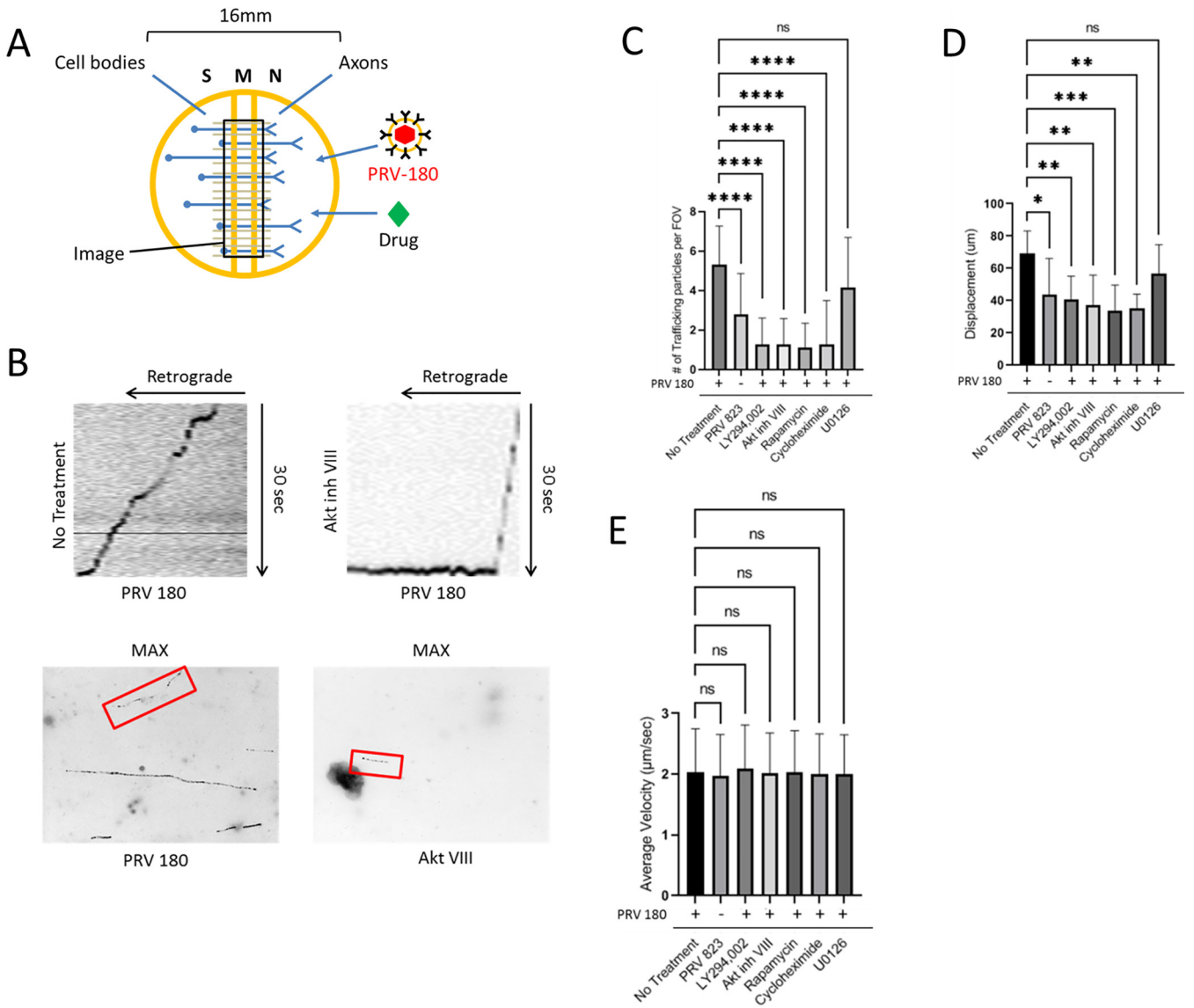


FIG 3 Quantification of PRV transport kinetics in axons. (A) N compartments were infected with PRV 180 or PRV 823. At 2 hpi, 30-s videos of moving nucleocapsids in M compartments were recorded. Inhibitor was added to N compartments 1 h prior to infection when specified. (B) Maximum-intensity projections (bottom) were created from the videos to visualize nucleocapsid displacement. Moving nucleocapsids are represented as tracks in the image (red box). Kymographs (top) were made from the maximum-intensity projections to visualize nucleocapsid velocity throughout the recording process. Diagonal lines starting from the upper right corner represent retrograde movement. Horizontal lines represent stationary nucleocapsids. (C) Quantification of the number of moving nucleocapsids in M compartments. (D) The displacement of individual nucleocapsids over the 30-s recordings were measured for each condition. (E) The average velocity of the nucleocapsids moving in the retrograde direction was calculated by acquiring the mean of all instantaneous velocities of $\geq 1 \mu\text{m/s}$. Data are means and SD for 7 chambers and 5 fields of view per chamber. ****, $P \leq 0.0001$, ***, $P \leq 0.001$, **, $P \leq 0.01$, and *, $P \leq 0.05$, using one-way ANOVA; ns, not significant.

Akt phosphorylation in axons requires PRV US3 Ser/Thr kinase. HSV-2 induces Akt phosphorylation upon binding of the glycoprotein B (gB) on the virion envelope with $\alpha_v\beta_3$ integrins, leading to release of intracellular calcium stores to promote entry of nucleocapsids into the cytoplasm (13). We wanted to determine if virion binding to the cell surface or fusion of the viral and cellular membranes was responsible for Akt phosphorylation and if Akt phosphorylation affected transport directly or indirectly by regulating entry of nucleocapsids into the cytoplasm.

N compartment axons were infected with PRV-Becker mutants lacking either glycoprotein D (gD) (PRV GS442) (38), the viral envelope protein required for specific PRV binding to the nectin-1 cell receptor, or gB (PRV 233) (39), the viral envelope protein required for fusion of the viral and cell membranes. Akt phosphorylation was

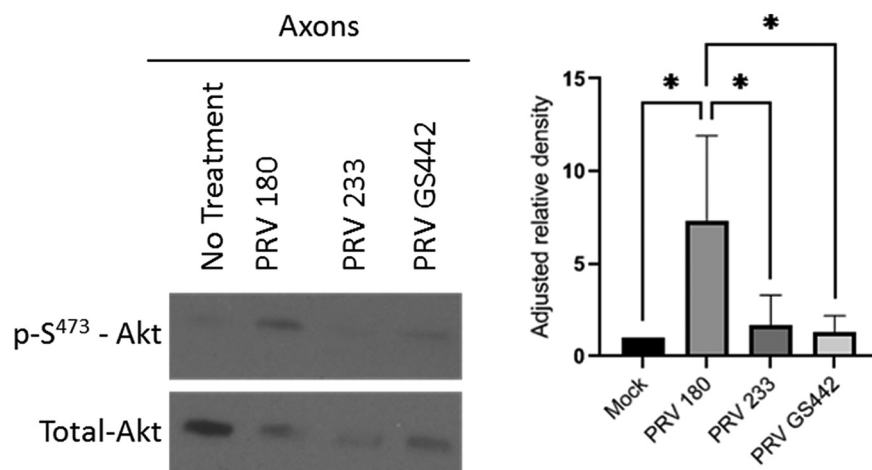


FIG 4 Akt phosphorylation in axons occurred after entry of PRV into the cytoplasm. Immunoblot of p-S⁴⁷³-Akt in axons infected with PRV 180, PRV 233, or PRV GS442 in N compartments. p-S⁴⁷³-Akt bands were normalized to total-Akt bands using a densitometry assay. Means and SD ($n = 3$) for each condition are plotted. *, $P \leq 0.05$, using one-way ANOVA.

monitored via Western blotting (Fig. 4) and was unchanged after infection with either of these mutants, suggesting that both binding and membrane fusion are required for Akt phosphorylation and that phosphorylation occurs at a downstream stage of infection.

To determine if Akt phosphorylation was promoted by PRV after entry into the cell, we investigated the role of US3. US3 is an AHV inner-tegument protein with Ser/Thr kinase function (20). US3 induces phosphorylation of Akt (in PRV) and downstream Akt substrates (in HSV-1) (15, 19). When we infected axons with a PRV-Becker mutant lacking US3 (PRV 813NS) (21) or a mutant lacking a functional kinase domain due to a K138A point mutation in the US3 catalytic domain (PRV 815KD) (40), no Akt phosphorylation was observed (Fig. 5). When axons were infected with a revertant of PRV 813NS, termed PRV 813R, Akt phosphorylation was restored (Fig. 5). These data indicate that US3 is responsible for promoting Akt phosphorylation after PRV infection in axons.

To determine if US3, and by extension Akt phosphorylation, is required for entry of PRV into cells, a PRV-Becker mutant strain containing an mRFP-VP26 fusion protein in a US3-null background (PRV 823) (21) was utilized. Rat fibroblasts (Rat2) were infected with either PRV 180 or PRV823 at a multiplicity of infection (MOI) of 5 at 4°C, a temperature permissive to binding but not entry. Cultures at 1 hpi were washed to remove inoculum, and the temperature was brought up to 37°C to allow entry. After 15 min, cells were washed with a low-pH citrate buffer (pH 3) to inactivate any unentered virus particles, and the infection was permitted to continue for another hour. Cells were fixed, and nucleocapsid fluorescence was visualized by fluorescence microscopy (Fig. 6). Nucleocapsids present within the cytoplasm were counted manually, and no significant difference was seen, indicating that US3 and Akt phosphorylation do not affect PRV entry in these cells and suggesting an entry mechanism different from what has been described for HSV-1 and HSV-2.

Next, we determined if US3 is required for efficient retrograde infection of neurons using the technique described for Fig. 2A. Compared to infection with PRV 180, infection with PRV 823 in axons led to an $\sim 44.7\% \pm 23.8\%$ reduction in dual-colored cell bodies in the S compartment (Fig. 2B). PRV 823 infection in axons in the N compartment also led to an $\sim 47.3\% \pm 38.4\%$ reduction in the number of trafficking nucleocapsids in the M compartment compared to PRV 180 (Fig. 3C). PRV 823 transport kinetics were comparable to those of PRV 180 when Akt-mTORC1 signaling or translation was disrupted (Fig. 3D and E); net displacement was significantly reduced ($\sim 37\% \pm 31.2\%$), but not transport velocity. These data correspond to a previous qualitative finding

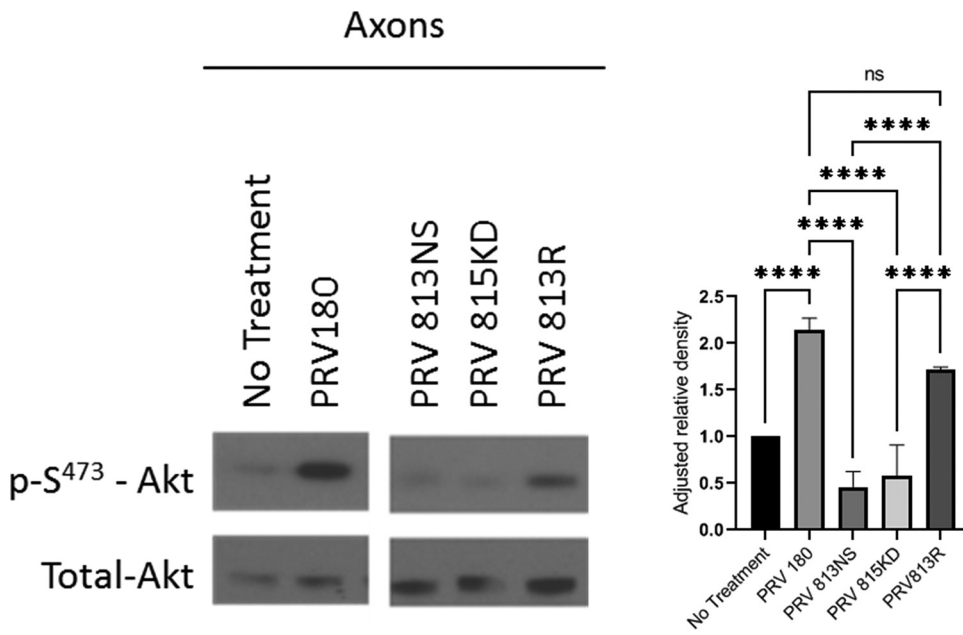


FIG 5 US3 induced Akt phosphorylation in axons. Immunoblot of p-S⁴⁷³-Akt in axons infected with PRV 180, PRV 813NS, PRV 815KD, or PRV 813R in N compartments. p-S⁴⁷³-Akt bands were normalized to total-Akt bands using a densitometry assay. Means and SD (*n* = 3) for each condition are plotted. ****, *P* ≤ 0.0001, using one-way ANOVA. The image was produced from cropped portions of a single membrane.

from our lab in which a reduction in the number of transporting nucleocapsids in axons as well as a reduction in the number of infected cell bodies after axonal infection was observed (21). Taken together, these data suggest that US3 mediates efficient retrograde transport of PRV nucleocapsids through axons by inducing an Akt-mTORC1 signaling pathway.

US3 and Akt phosphorylation are required for virus-induced local translation in axons. We directly tested whether US3 and Akt phosphorylation were required for translation by performing a SUnSET (surface sensing of translation) assay. Axons in the N compartment were either untreated or treated with Akt inhibitor VIII, cycloheximide, or U0126 and then infected with PRV 180 or PRV 813NS. Puromycin was added to both N and S compartments to label nascent peptides 15 min prior to harvesting for Western blotting (Fig. 7A). Nascent peptides were visualized using a monoclonal puro-

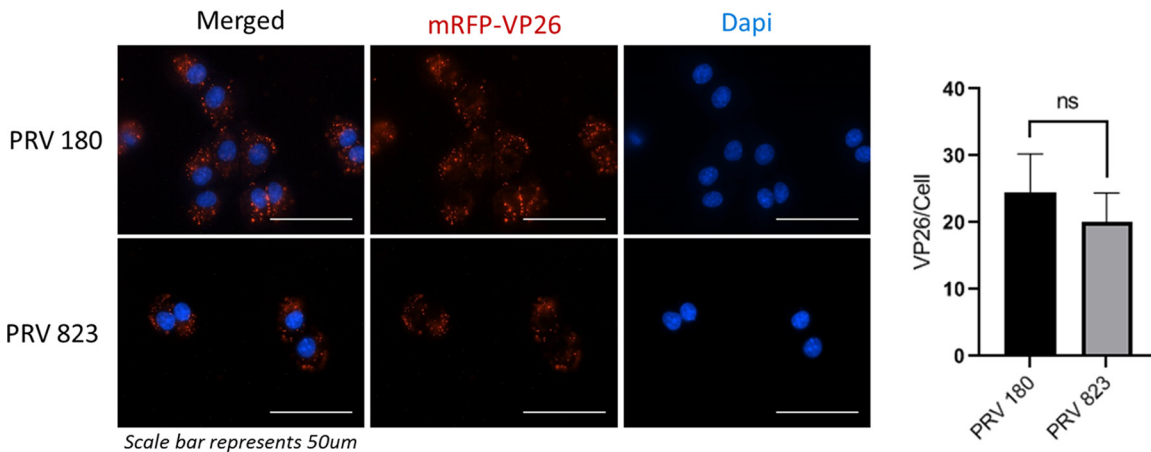


FIG 6 US3 does not affect entry of PRV into cells. Fluorescence imaging of PRV 180 and PRV 823 nucleocapsids in Rat2 fibroblasts. A synchronized infection assay was used to allow entry of all bound virion particles to occur simultaneously. Nucleocapsids that entered the cytoplasm were manually counted. Data are means and SD, with 5 replicates and 2 to 5 cells per replicate for each condition. ns, not significant using an unpaired *t* test.

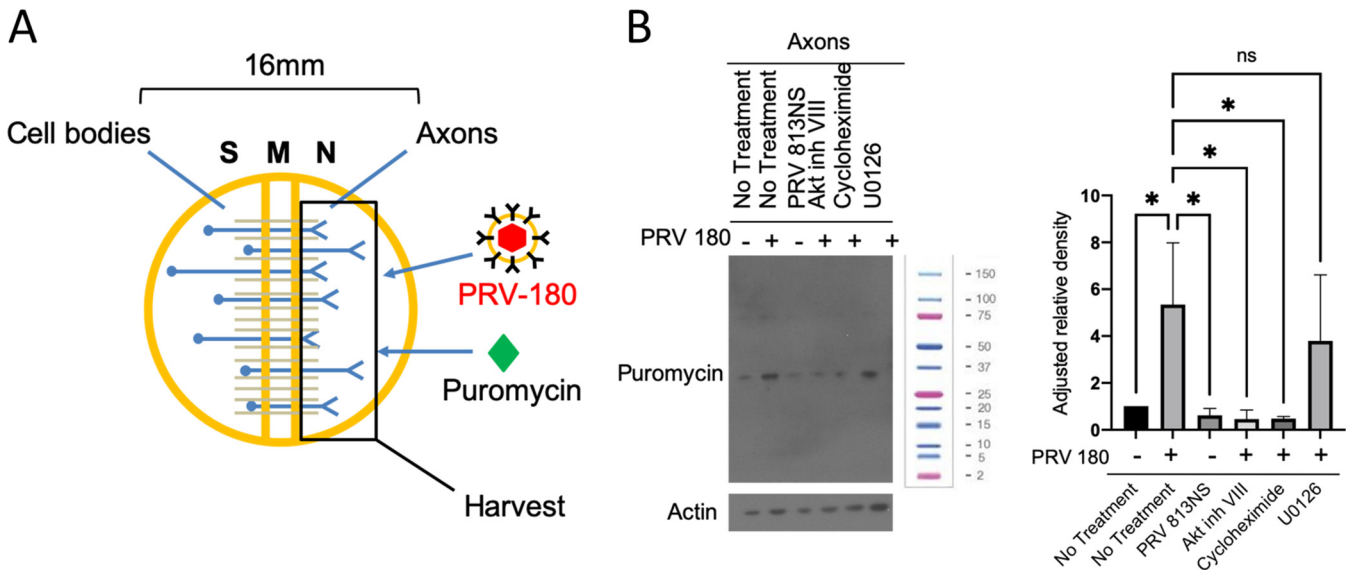


FIG 7 US3 and Akt phosphorylation are required for virus-induced translation in axons. (A) N compartments were infected with PRV 180 for 1 h prior to harvest. Puromycin was added to N compartments at 45 mpi to label nascent peptides. (B) Immunoblot of puromycin-incorporated peptides from axons in the N compartment. PRV 180 or PRV 813NS were added to N compartments for 1 h. Puromycin was added to N compartments 45 mpi. Inhibitor was added 1 h prior to infection when specified. A single band is visible for each condition in this blot, representing the most abundant peptide synthesized at the time of incubation. Other peptide bands become visible at higher exposure times. The molecular weight ladder shown is a Bio-Rad Precision Plus protein standard (1610374).

mycin antibody. Infection of axons with PRV 180 but not PRV 813NS led to a significant increase in puromycin incorporation compared to mock infection, indicating that US3 is required for PRV-mediated translation in axons. When Akt phosphorylation and translation were inhibited, no significant increase in puromycin incorporation occurred. Pretreatment with U0126 had no effect on puromycin incorporation, suggesting that the Ras/MAPK pathway does not affect PRV-induced translation in axons (Fig. 7B).

DISCUSSION

PNS neurons are highly polarized, with axon terminals extending centimeters away from their cell bodies. Accordingly, the transport of molecular messengers over these long distances is highly regulated (41). Axons contain within them the complete set of protein synthesis machinery, including multiple subsets of localized mRNA that are used to synthesize proteins in response to changes in the extracellular environment and send messages to the cell body to produce a global response to stimuli (42, 43). PRV hijacks these processes to promote its efficient retrograde transport from the site of infection, in the axon, to the cell body (10). In this study, we have discovered that PRV utilizes an Akt-mToRC1 signaling pathway to induce translation in axons at early time points after infection. The inner-tegment protein kinase US3 is required for the induction of this signaling pathway and acts upstream of PI3K to promote Akt phosphorylation (Fig. 8).

Infection of axons with PRV 180 in the presence of the PI3K inhibitor LY294002 significantly reduced the number of moving nucleocapsids (Fig. 3C) and reduced the distance nucleocapsids traveled before stopping (Fig. 3D). US3 must act upstream of PI3K to promote efficient transport, but it is unknown if PI3K is the direct kinase target of US3. Earlier studies have shown that US3 is responsible for the reorganization of the actin cytoskeleton via cofilin activation (6). US3 interacts directly with group 1 PAKs (p-21 activated kinases) to promote cofilin dephosphorylation (activation), leading to disassembly of filamentous actin and the entry of virion tegument and nucleocapsid into the cytoplasm (44). Group 1 PAKs play an important role in cytoskeleton rearrangement and apoptosis signal transduction (45–52) and have been shown to interact with various members of PI3K and Akt signaling pathways (53). It is possible that the cross

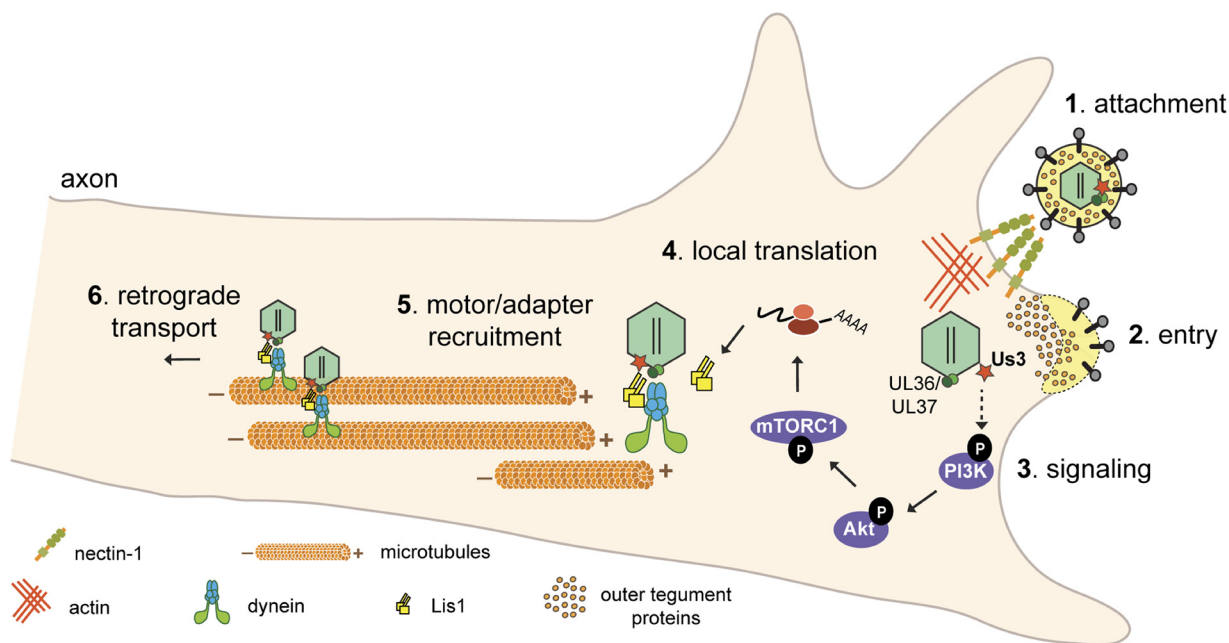


FIG 8 Model for PRV-induced translation in axons. (Step 1) PRV virions bind to nectin-1 receptors on the host cell membrane. (Step 2) Entry is mediated by fusion of the viral envelope with the cell's plasma membrane, allowing nucleocapsid and tegument proteins to enter the cytoplasm. Inner tegument proteins (US3, UL36, and UL37) stay bound to nucleocapsids. (Step 3) US3 stimulates a PI3K/Akt-mTORC1 signaling pathway either directly or indirectly (the dashed arrow indicates that the direct kinase target is still unknown) to induce translation of axonal mRNAs leading to Lis1 expression (step 4). (Steps 5 and 6) Nucleocapsid engagement with the retrograde transport machinery is mediated by the inner tegument and Lis1 (step 5), and subsequent retrograde transport through the axon occurs (step 6).

talk between group 1 PAKs and the PI3K-Akt signaling pathway could be utilized by US3 to promote cytoskeletal rearrangements and local translation.

When US3 was absent or PI3K/Akt-mTORC1 signaling was disrupted, we observed a significant reduction in the number of transporting nucleocapsids and their processivity (Fig. 3). Under these conditions, nucleocapsids moved shorter distances before stopping; however, the velocity of these nucleocapsids while in motion was similar to that seen in wild-type infection without inhibitor present. This suggests that nucleocapsids had difficulty engaging with the transport machinery rather than difficulty transporting once engaged. These results were similar to what was seen for PRV and HSV-1 mutants when the R2 domain of the UL37 inner-tegument protein was altered (4). The UL37-R2 mutant replicates well in peripheral tissue but is unable to move efficiently in peripheral neurons. As a result, the mutant cannot establish lifelong infection in the host, a property that would provide a new possibility for vaccine design (4). Due to the reduced transport efficiency of the US3-null PRV mutant as well as the UL37-R2 mutant, it is possible that a PRV mutant which both is null for US3 and has the UL37-R2 mutation may provide a similar or additive effect by further reducing the chance of retrograde infection in peripheral neurons.

Long-distance transport in axons requires the microtubule network and associated motor proteins. The kinesin motor proteins mediate anterograde (plus-end-directed) transport, and dynein motor proteins mediate retrograde (minus-end-directed) transport (54). Dynein is a multisubunit complex composed of two heavy chains, two intermediate chains, and two light chains that regulate motor activity and interactions with cellular cargo (55–58). To achieve spatiotemporal regulation of transport, various accessory factors associate with the dynein complex; one such factor is dynactin (54). The UL36 inner-tegument protein interacts with dynactin to recruit nucleocapsids to dynein (8, 9); however, this interaction alone is not sufficient to promote efficient transport. Dynein must be phosphorylated to obtain an active conformation (54, 55, 59–61). Recently, it was shown that upon infection of epithelial cells with HSV-1, dynein

intermediate chain 1B was phosphorylated at position S80 in an Akt- and protein kinase C (PKC)-independent manner (62). It was speculated that US3's kinase function could mediate the activation of dynein throughout the retrograde transport process. More work needs to be done to determine the cause and function of dynein phosphorylation during AHV infection.

Axonal infection with PRV mutants lacking either gD or gB, the glycoproteins that mediate virion binding to the plasma membrane and carry out membrane fusion, was unable to stimulate Akt phosphorylation (Fig. 4). These observations suggested that Akt is phosphorylated after entry of the nucleocapsid and tegument proteins in the cytoplasm. These findings are different from what was observed after HSV-1 and HSV-2 infection. Infection with these AHVs leads to the stimulation of a low-level Ca^{2+} fluctuation following binding of gD or gB to the nectin-1 coreceptor and heparin sulfate proteoglycans on the cell surface. This is followed by an interaction between Akt and gB leading to Akt phosphorylation, a larger Ca^{2+} fluctuation and entry of the nucleocapsid and tegument into the cytoplasm (13). We have shown that PRV nucleocapsid entry does not depend on US3 and, by extension, Akt phosphorylation (Fig. 6). However, we have not investigated the potential for the induction of Ca^{2+} fluctuation during infection and whether it participates in the retrograde transport process. Future work needs to be done to determine the effects of Ca^{2+} signaling in PRV infection.

Our work has revealed a novel role for US3 in the promotion of efficient microtubule-based transport of PRV nucleocapsids in axons. We determined that US3 signals through an Akt-mTORC1 signaling pathway, upstream of PI3K, to induce translation of localized, repressed mRNAs, a process required for efficient retrograde transport. The absence of US3 or the disruption of Akt-mTORC1 not only reduced the number of transporting nucleocapsids but also negatively impacted the processivity of nucleocapsids moving through the axon, suggesting that engagement with the dynein-motor complex was disrupted. This work helps to clarify the viral and cellular factors involved in PRV entry and retrograde transport in axons and identifies US3 as a potential target for therapies aiming to prevent the spread of AHVs in the nervous system.

MATERIALS AND METHODS

Primary neuronal culture. Superior cervical ganglion (SCG) neurons were isolated from embryonic day 17 Sprague-Dawley rat embryos and cultured as previously described (30). Briefly, SCG were trypsinized and mechanically dissociated. Thirty-five-millimeter cell culture dishes were coated with poly-DL-ornithine (Sigma-Aldrich) and laminin (Invitrogen) and then fitted with a Campenot trichamber (CAMP320 isolator rings; Tyler Research) using autoclaved silicone vacuum grease as an adherent. Dissociated SCG were seeded in one compartment (the S-compartment) of the trichamber filled with neurobasal medium (Life Technologies; 21103049) plus $50\times$ B-27 supplement (Life Technologies; 17504044), $100\times$ penicillin-streptomycin-glutamine (Thermo Fisher; 10378016) and 80 ng/mL NGF (Nerve Growth Factor) (Thermo Fisher; 13257019) and left to grow for ~ 3 weeks with medium changes every 7 days.

Cell lines and virus stocks. Porcine kidney epithelial cells (PK15; ATCC) and Rat2 cells (ATCC) were maintained in Dulbecco modified Eagle medium (DMEM; HyClone) with 10% fetal bovine serum (FBS, HyClone) and 1% penicillin-streptomycin (HyClone). Virus propagation and titration were performed in PK15 cells unless otherwise specified. Rat2 cells were used for synchronized infection assays. LP cells (gB-complementing cells derived from PK15 cells) were used to grow gB-complemented PRV 233 virus stocks (L. Pomeranz, personal communication). Geneticin (G418; 100 $\mu\text{g}/\text{mL}$) (InvivoGen; ant-gn-1) was added to culture every fifth passage to maintain gB expression. G5 cells (gD-complementing cells derived from PK15 cells) were used to grow gD-complemented PRV GS442 virus stocks (38). 2.5 mM L-histidinol dihydrochloride (Sigma; H6647) was added to cultures every 5th passage to maintain gD expression. Noncomplemented versions of PRV 233 and PRV GS442 were produced through infection of PK15 cells with the phenotypically complemented versions of each strain. To normalize the amount of PRV 233 and PRV GS442 used, the genome to PFU ratio of the complemented version of each strain was used to approximate the "theoretical PFU" of the noncomplemented strain. All cells were incubated at 37°C and 5% CO_2 .

Unless otherwise specified, virus infections of PK15 and Rat2 cells were performed with 10^6 PFU of virus in DMEM plus 2% FBS. Titers of virus stocks were determined as PFU. For live-cell imaging PRV 180 and PRV 823 stocks were used within 2 weeks of production for no more than one freeze-thaw cycle to preserve the fluorophore intensity. Virus stocks used are shown in Table 1.

Antibodies and chemicals. All antibodies were diluted in TBS-T (Tris-buffered saline-Tween; 0.1%) treated with 3% bovine serum albumin (BSA) and stored at -20°C unless otherwise specified. Rabbit phospho-Akt (ser473) (D9E) (Cell Signaling Technology; 4060) was used at 1:1,000 for Western blotting (WB). Rabbit Akt antibody (Cell Signaling Technology; 9272) was used at 1:1,000 to detect total Akt in

TABLE 1 Virus stocks

Virus strain	Genotype	Reference
PRV 180	Becker wild-type strain with mRFP-VP26 fusion	64
PRV 813NS	US3-null Becker strain; nonsense mutation; does not contain mRFP-VP26 fusion	21
PRV 815KD	US3 kinase-dead Becker strain; K138A point mutation; does not contain mRFP-VP26 fusion	40
PRV 813R	Revertant of 813NS; does not contain mRFP-VP26 fusion	21
PRV 823	US3-null Becker strain; does contain mRFP-VP26 fusion	21
PRV GS442	gD-null Becker strain; diffusible GFP expression	38
PRV 233	gB-null Becker strain; diffusible GFP expression	39

WB. Monoclonal anti-beta-actin antibody (Sigma-Aldrich; A1978) was used at 1:10,000 for WB. Mouse monoclonal US3 7H10.21 (21) was used at 1:1,000 for WB. Mouse monoclonal anti-puromycin clone 4G11 (EMD Millipore; MABE342) was used at 1:2,000 for WB.

All drug treatments occurred 1 h prior to infection, concentrations represent final experimental concentrations, and drugs were resuspended in dimethyl sulfoxide (DMSO) unless otherwise specified. LY294002 (Cell Signaling Technology; 9901) was used at a concentration of 20 μ M. Akt inhibitor VIII (Sigma; 124018) was used at a concentration of 5 μ M. Rapamycin (Sigma; 553210) was used at a concentration of 100 μ M. U0126 (Sigma; 662009) was used at a concentration of 10 μ M. Puromycin (AG Scientific; P-1033-SOL) was solubilized in deionized H₂O and used at a concentration of 1 μ g/mL. FAST-DiO (Thermo Fisher; D3898) was used a concentration of 5 μ g/mL and incubated for 12 h prior to infection (24 h prior to imaging).

Western blotting. SCG neurons in trichambers were seeded at a density of 1 SCG per S compartment. Dishes were washed three times with warm phosphate-buffered saline (PBS) and then incubated with neurobasal medium plus 100 \times penicillin-streptomycin-glutamine (note the lack of B-27 supplement) for 12 h prior to infection. Either axons in the N compartment or cell bodies in the S compartment were lysed in the chamber with 40 μ l of 2 \times Laemmli buffer prepared from a dilution of 5 \times Laemmli buffer (10% SDS, 300 mM Tris-Cl [pH 6.8], 0.05% bromophenol blue, 100 mM dithiothreitol [DTT], and 50% glycerol in double-distilled water [ddH₂O]). Lysates were boiled at 90°C for 5 min and then cooled on ice. Proteins were separated by SDS-PAGE and 4 to 12% gradient NuPAGE bis-Tris gels. Proteins were transferred to nitrocellulose membranes (GE Healthcare; 45-0040002) using a Trans-Blot SD semidry transfer cell (Bio-Rad). Membranes were blocked using 1 \times Pierce clear milk blocking buffer (Thermo Fisher; 37587) for 30 min at room temperature (RT) and then washed three times with TBS-T. Membranes were incubated in primary antibody dilution overnight at 4°C followed by three TBS-T washes, incubation with horseradish peroxidase-conjugated secondary antibody (1:10,000 dilutions in 3% BSA-TBS-T) for 45 min at RT, and a final three washes with TBS-T. The chemiluminescent substrate SuperSignal West Pico (Thermo Fisher; 34080), West Dura extended-duration substrate (Thermo Fisher; 34075), West Femto maximum-sensitivity substrate (Thermo Fisher; 34094), or West Atto ultimate-sensitivity substrate (Thermo Fisher; A38554) was added to the membranes for 5 min at RT. Protein bands were visualized by exposing the membranes on HyBlot CL autoradiography film (Denville Scientific; E3018).

SUnSET assay for labeling nascent peptides. Puromycin was added to the chamber compartment to be analyzed 15 min prior to harvest. The rest of the protocol follows the same as for WB. Puromycin-labeled peptides were detected with puromycin antibodies. See “Antibodies and chemicals” for the primary antibody used.

Synchronized infection assay. Rat2 cells in culture were cooled to 4°C. PRV 180 or PRV823 inocula were added at an MOI of 5, and virion absorption to cells was allowed to occur for 1 h at 4°C before medium was aspirated and cells were washed with chilled PBS three times. Chilled 2% FBS-DMEM was added to the dish, and the temperature was brought up to 37°C for 15 min to enable virion entry. Medium was removed, and infected cells were washed once with a low-pH citrate buffer for 2 min to inactivate virions that had not entered cells. Citrate buffer was removed, and cells were washed three times with PBS at RT before warm 2% FBS-DMEM was added. Infected cells were incubated for 1 h at 37°C.

Cells were fixed using 4% paraformaldehyde (PFA) for 10 min at RT and permeabilized with 0.1% Triton X-100 (Sigma; T8787) for 10 min at RT. After permeabilization, plates were blocked for 1 h at RT with 1% BSA in PBS, washed three times with PBS, and then treated with DAPI (4',6-diamidino-2-phenylindole; Thermo Fisher; 62248) to stain cell nuclei for 5 min at RT in the dark with 1 μ g/mL DAPI in 0.1% BSA-PBS. Cells were washed three times with PBS and then imaged. Total and average numbers of red fluorescent nucleocapsids per cell in a single field of view (FOV) were manually counted using NIS Elements Advanced Research software (Nikon).

Retrograde transport assay. SCGs were seeded at 2/3 of an SCG per S compartment. Fast-DiO was added to axons in the N compartment 12 h prior to infection. N compartments were either untreated or treated with LY294002, Akt inhibitor VIII, rapamycin, cycloheximide, or U0126 1 h prior to infection. Axons in N compartments were infected with 10⁶ PFU of PRV. At 6 h postinfection, unabsorbed virus inoculum and drug in the N compartment were washed out and replaced with fresh neurobasal medium. At 12 h postinfection, cell bodies in the S compartment were tile imaged for mRFP-VP26 (red) and DiO (green). Total numbers of green and dual-colored particles (red and green) were manually counted (see “Synchronized infection assay”). The ratio of dual-colored cell bodies to total green cell bodies was determined per S compartment and averaged for all conditions.

Single-particle tracking in trichambers. SCGs were seeded at 2/3 of an SCG per S compartment with optical plastic tissue culture dishes (Ibidi; 81156-400). N-compartment axons were either untreated

or treated with drug for 1 h prior to infection. Infections were initiated at 10^6 PFU for 2 h before time-lapse imaging was used to visualize moving fluorescent virus particles in the M compartment. Thirty-second recordings of a single FOV were completed at approximately 2 frames per s. The total number of moving virus particles were counted. For instantaneous velocity measurements, the TrackMate plug-in for ImageJ was used. Velocities were parsed into bins in a histogram ranging from $-4 \mu\text{m/s}$ (the maximum anterograde velocity recorded) and $+4 \mu\text{m/s}$ (the maximum retrograde velocity recorded) with intervals of $1 \mu\text{m/s}$. Instantaneous velocities in bins $1 \mu\text{m/s}$ to $4 \mu\text{m/s}$ were averaged across all conditions to determine the average velocity of all moving virion particles. Velocities in the $0\text{-}\mu\text{m/s}$ bin were assumed to be stationary particles and were not included in the average velocity measurements.

Imaging processing and analysis. All imaging was conducted on a Nikon Eclipse Ti inverted epifluorescence microscope using a CoolSNAP ES2 charge-coupled device (CCD) camera. Images and movies were processed using ImageJ (63) and NIS Elements Advanced Research software (Nikon). Comparative images were all captured with the same exposure times; brightness and contrast adjustments were applied to the entire image; and alterations were applied equally across conditions.

To analyze trafficking virus particles in the M compartment, ImageJ was used to create maximum-intensity projections of all videos to visualize the path of moving particles. Particle trajectories were manually counted and taken to represent a single moving particle. The directionality and velocity of a moving particle was visualized using the ImageJ multi kymograph tool. Particle lengths were calculated by measuring the total particle distance traveled over the course of the 30-s movie using the segmented line tool in ImageJ. In order to be counted, particles must not enter or exit the FOV during the entire 30-s recording time.

Statistical analysis. All data were analyzed using GraphPad Prism 9 (GraphPad Software, La Jolla, California, USA). Figure legends provide the statistical test used for each analysis.

ACKNOWLEDGMENTS

This work was supported by U.S. National Institutes of Health grant (5R37NS033506) to Lynn W. Enquist.

We thank Heath E. Johnson for assistance with particle tracking automation.

We declare that we have no competing interests.

REFERENCES

- Pomeranz LE, Reynolds AE, Hengartner CJ. 2005. Molecular biology of pseudorabies virus: impact on neurovirology and veterinary medicine. *Microbiol Mol Biol Rev* 69:462–500. <https://doi.org/10.1128/MMBR.69.3.462-500.2005>.
- Döhner K, Wolfstein A, Prank U, Echeverri C, Dujardin D, Vallee R, Sodeik B. 2002. Function of dynein and dynactin in herpes simplex virus capsid transport. *Mol Biol Cell* 13:2795–2809. <https://doi.org/10.1091/mbc.01-07-0348>.
- Sodeik B, Ebersold M, Helenius A. 1997. Microtubule-mediated transport of incoming herpes simplex virus 1 capsids to the nucleus. *J Cell Biol* 136:1007–1021. <https://doi.org/10.1083/jcb.136.5.1007>.
- Richards AL, Sollars PJ, Pitts JD, Stults AM, Heldwein EE, Pickard GE, Smith GA. 2017. The pUL37 tegument protein guides alpha-herpesvirus retrograde axonal transport to promote neuroinvasion. *PLoS Pathog* 13:e1006741. <https://doi.org/10.1371/journal.ppat.1006741>.
- Sekine E, Schmidt N, Gaboriau D, O'Hare P. 2017. Spatiotemporal dynamics of HSV genome nuclear entry and compaction state transitions using bioorthogonal chemistry and super-resolution microscopy. *PLoS Pathog* 13:e1006721. <https://doi.org/10.1371/journal.ppat.1006721>.
- Jacob T, Van den Broeke C, van Troys M, Waterschoot D, Ampe C, Favoreel HW. 2013. Alphaherpesviral US3 kinase induces cofilin dephosphorylation to reorganize the actin cytoskeleton. *J Virol* 87:4121–4126. <https://doi.org/10.1128/JVI.03107-12>.
- Jovasevic V, Naghavi MH, Walsh D. 2015. Microtubule plus end-associated CLIP-170 initiates HSV-1 retrograde transport in primary human cells. *J Cell Biol* 211:323–337. <https://doi.org/10.1083/jcb.201505123>.
- Radtke K, Kienke D, Wolfstein A, Michael K, Steffen W, Scholz T, Karger A, Sodeik B. 2010. Plus- and minus-end directed microtubule motors bind simultaneously to herpes simplex virus capsids using different inner tegument structures. *PLoS Pathog* 6:e1000991. <https://doi.org/10.1371/journal.ppat.1000991>.
- Zaichick SV, Bohannon KP, Hughes A, Sollars PJ, Pickard GE, Smith GA. 2013. The herpesvirus VP1/2 protein is an effector of dynein-mediated capsid transport and neuroinvasion. *Cell Host Microbe* 13:193–203. <https://doi.org/10.1016/j.chom.2013.01.009>.
- Koyuncu O, Perlman D, Enquist LW. 2013. Efficient retrograde transport of pseudorabies virus within neurons requires local protein synthesis in axons. *Cell Host Microbe* 13:54–66. <https://doi.org/10.1016/j.chom.2012.10.021>.
- Sonenberg N, Hinnebusch A. 2009. Regulation of translation initiation in eukaryotes: mechanisms and biological targets. *Cell* 136:731–745. <https://doi.org/10.1016/j.cell.2009.01.042>.
- Cheshenko N, Liu W, Satlin LM, Herold BC. 2007. Multiple receptor interactions trigger release of membrane and intracellular calcium stores critical for herpes simplex virus entry. *Mol Biol Cell* 18:3119–3130. <https://doi.org/10.1091/mbc.e07-01-0062>.
- Cheshenko N, Trepanier JB, González PA, Eugenin EA, Jacobs WR, Herold BC. 2014. Herpes simplex virus type 2 glycoprotein H interacts with integrin $\alpha\text{v}\beta\text{3}$ to facilitate viral entry and calcium signaling in human genital tract epithelial cells. *J Virol* 88:10026–10038. <https://doi.org/10.1128/JVI.00725-14>.
- Benetti L, Roizman B. 2006. Protein kinase B/Akt is present in activated form throughout the entire replicative cycle of $\Delta\text{U}_5\text{3}$ mutant virus but only at early times after infection with wild-type herpes simplex virus 1. *J Virol* 80:3341–3348. <https://doi.org/10.1128/JVI.80.7.3341-3348.2006>.
- Chuluunbaatar U, Mohr I. 2011. A herpesvirus kinase that masquerades as Akt: you don't have to look like Akt, to act like it. *Cell Cycle* 10:2064–2068. <https://doi.org/10.4161/cc.10.13.16242>.
- Liu X, Cohen J. 2013. Varicella-zoster virus ORF12 protein activates the phosphatidylinositol 3-kinase/Akt pathway to regulate cell cycle progression. *J Virol* 87:1842–1848. <https://doi.org/10.1128/JVI.02395-12>.
- Sen N, Mukherjee G, Sen A, Bendall SC, Sung P, Nolan G, Arvin AM. 2014. Single-cell mass cytometry analysis of human tonsil T cell remodeling by varicella zoster virus. *Cell Rep* 8:633–645. <https://doi.org/10.1016/j.celrep.2014.06.024>.
- Rahaus M, Desloges N, Wolff MH. 2007. Varicella-zoster virus requires a functional PI3K/Akt/GSK-3 α /beta signaling cascade for efficient replication. *Cell Signal* 19:312–320. <https://doi.org/10.1016/j.cellsig.2006.07.003>.
- Chang CD, Lin PY, Liao MH, Change CI, Hsu JL, Yu FL, Wu HY, Shih WL. 2013. Suppression of apoptosis by pseudorabies virus US3 protein kinase through the activation of PI3-K/Akt and NF- κ B pathways. *Res Vet Sci* 95:764–774. <https://doi.org/10.1016/j.rvsc.2013.06.003>.
- Deruelle M, Favoreel H. 2011. Keep it in the subfamily: the conserved alphaherpesvirus US3 protein kinase. *J Gen Virol* 92:18–30. <https://doi.org/10.1099/vir.0.025593-0>.

21. Olsen LM, Ch'ng TH, Card JP, Enquist LW. 2006. Role of pseudorabies virus Us3 protein kinase during neuronal infection. *J Virol* 80:6387–6398. <https://doi.org/10.1128/JVI.00352-06>.
22. Frame M, Purves FC, McGeoch DJ, Marsden HS, Leader DP. 1987. Identification of the herpes simplex virus protein kinase as the product of viral gene US3. *J Gen Virol* 68:2699–2704. <https://doi.org/10.1099/0022-1317-68-10-2699>.
23. Hanks S, Quinn AM, Hunter T. 1988. The protein kinase family: conserved features and deduced phylogeny of the catalytic domains. *Science* 241:42–52. <https://doi.org/10.1126/science.3291115>.
24. Heineman TC, Seidel K, Cohen JL. 1996. The varicella-zoster virus ORF66 protein induces kinase activity and is dispensable for viral replication. *J Virol* 70:7312–7317. <https://doi.org/10.1128/JVI.70.10.7312-7317.1996>.
25. McGeoch D, Davison A. 1986. Alphaherpesviruses possess a gene homologous to the protein kinase gene family of eukaryotes and retroviruses. *Nucleic Acids Res* 14:1765–1777. <https://doi.org/10.1093/nar/14.4.1765>.
26. Purves F, Longnecker RM, Leader DP, Roizman B. 1987. Herpes simplex virus 1 protein kinase is encoded by open reading frame US3 which is not essential for virus growth in cell culture. *J Virol* 61:2896–2901. <https://doi.org/10.1128/JVI.61.9.2896-2901.1987>.
27. Brzozowska A, Rychłowski M, Lipińska AD, Bieńkowska-Szewczyk K. 2010. Point mutations in BHV-1 Us3 gene abolish its ability to induce cytoskeletal changes in various cell types. *Vet Microbiol* 143:8–13. <https://doi.org/10.1016/j.vetmic.2010.02.008>.
28. Granstedt AE, Bosse JB, Thiberge SY, Enquist LW. 2013. In vivo imaging of alphaherpesvirus infection reveals synchronized activity dependent on axonal sorting of viral proteins. *Proc Natl Acad Sci U S A* 110:E3516–E3525. <https://doi.org/10.1073/pnas.1311062110>.
29. Mettenleiter T, Klupp BG, Granzow H. 2009. Herpesvirus assembly: an update. *Virus Res* 143:222–234. <https://doi.org/10.1016/j.virusres.2009.03.018>.
30. Curanović D, Ch'ng TH, Szpara M, Enquist L. 2009. Compartmented neuron cultures for directional infection by alpha herpesviruses. *Curr Protoc Cell Biol* Chapter 26:Unit 26.4. <https://doi.org/10.1002/0471143030.cb2604s43>.
31. Chan T, Rittenhouse S, Tschlis P. 1999. AKT/PKB and other D3 phosphoinositide-regulated kinases: kinase activation by phosphoinositide-dependent phosphorylation. *Annu Rev Biochem* 68:965–1014. <https://doi.org/10.1146/annurev.biochem.68.1.965>.
32. Ballif BA, Roux PP, Gerber SA, MacKeigan JP, Blenis J, Gygi SP. 2005. Quantitative phosphorylation profiling of the ERK/p90 ribosomal S6 kinase-signaling cassette and its targets, the tuberous sclerosis tumor suppressors. *Proc Natl Acad Sci U S A* 102:667–672. <https://doi.org/10.1073/pnas.0409143102>.
33. Carriere A, Romeo Y, Acosta-Jaquez HA, Moreau J, Bonneil E, Thibault P, Fingar DC, Roux PP. 2011. ERK1/2 phosphorylate raptor to promote Ras-dependent activation of mTOR complex 1 (mTORC1). *J Biol Chem* 286:567–577. <https://doi.org/10.1074/jbc.M110.159046>.
34. Hassan B, Akcakanat A, Holder AM, Meric-Bernstam F. 2013. Targeting the PI3-kinase/Akt/mTOR signaling pathway. *Surg Oncol Clin N Am* 22:641–664. <https://doi.org/10.1016/j.soc.2013.06.008>.
35. Hemmings B, Restuccia D. 2012. PI3K-PKB/Akt pathway. *Cold Spring Harb Perspect Biol* 4:a011189. <https://doi.org/10.1101/cshperspect.a011189>.
36. Ma L, Chen Z, Erdjument-Bromage H, Tempst P, Pandolfi PP. 2005. Phosphorylation and functional inactivation of TSC2 by Erk implications for tuberous sclerosis and cancer pathogenesis. *Cell* 121:179–193. <https://doi.org/10.1016/j.cell.2005.02.031>.
37. Roux P, Ballif BA, Anjum R, Gygi SP, Blenis J. 2004. Tumor-promoting phorbol esters and activated Ras inactivate the tuberous sclerosis tumor suppressor complex via p90 ribosomal S6 kinase. *Proc Natl Acad Sci U S A* 101:13489–13494. <https://doi.org/10.1073/pnas.0405659101>.
38. Peeters B, de Wind N, Broer R, Gielkens A, Moormann R. 1992. Glycoprotein H of pseudorabies virus is essential for entry and cell-to-cell spread of the virus. *J Virol* 66:3888–3892. <https://doi.org/10.1128/JVI.66.6.3888-3892.1992>.
39. Curanovic D, Enquist LW. 2009. Virion-incorporated glycoprotein B mediates transneuronal spread of pseudorabies virus. *J Virol* 83:7796–7804. <https://doi.org/10.1128/JVI.00745-09>.
40. Olsen LM. Functions of protein kinase Us3 in the PRV life cycle. Thesis. Princeton University, Princeton, NJ.
41. Holt CE, Martin KC, Schuman EM. 2019. Local translation in neurons: visualization and function. *Nat Struct Mol Biol* 26:557–566. <https://doi.org/10.1038/s41594-019-0263-5>.
42. Merianda TT, Lin AC, Lam JSY, Vuppalandi D, Willis DE, Karin N, Holt CE, Twiss JL. 2009. A functional equivalent of endoplasmic reticulum and Golgi in axons for secretion of locally synthesized proteins. *Mol Cell Neurosci* 40:128–142. <https://doi.org/10.1016/j.mcn.2008.09.008>.
43. Murashov AK, Chintalgattu V, Islamov RR, Lever TE, Pak ES, Sierpinski PL, Katwa LC, Van Scott MR. 2007. RNAi pathway is functional in peripheral nerve axons. *FASEB J* 21:656–670. <https://doi.org/10.1096/fj.06-6155com>.
44. Van den Broeke C, Radu M, Deruelle M, Nauwynck H, Hofmann C, Jaffer ZM, Chernoff J, Favoreel HW. 2009. Alphaherpesvirus US3-mediated reorganization of the actin cytoskeleton is mediated by group A p21-activated kinases. *Proc Natl Acad Sci* 106:8707–8712. <https://doi.org/10.1073/pnas.0900436106>.
45. Frost JA, Swantek JL, Stippec S, Yin MJ, Gaynor R, Cobb MH. 2000. Stimulation of NFκB activity by multiple signaling pathways requires PAK1. *J Biol Chem* 275:19693–19699. <https://doi.org/10.1074/jbc.M909860199>.
46. Bagrodia S, Dé Rijard B, Davis RJ, Cerione RA. 1995. Cdc42 and PAK-mediated signaling leads to Jun kinase and p38 mitogen-activated protein kinase activation. *J Biol Chem* 270:27995–27998. <https://doi.org/10.1074/jbc.270.47.27995>.
47. Zhang S, Han J, Sells MA, Chernoff J, Ulevitch RJ, Bokoch GM. 1995. Rho family GTPases regulate p38 mitogen-activated protein kinase through the downstream mediator Pak1. *J Biol Chem* 270:23934–23936. <https://doi.org/10.1074/jbc.270.41.23934>.
48. Polverino A, Frost J, Yang P, Hutchison M, Neiman AM, Cobb MH, Marcus S. 1995. Activation of mitogen-activated protein kinase cascades by p21-activated protein kinases in cell-free extracts of *Xenopus* oocytes. *J Biol Chem* 270:26067–26070. <https://doi.org/10.1074/jbc.270.44.26067>.
49. Sells MA, Knaus UG, Bagrodia S, Ambrose DM, Bokoch GM, Chernoff J. 1997. Human p21-activated kinase (Pak1) regulates actin organization in mammalian cells. *Curr Biol* 7:202–210. [https://doi.org/10.1016/s0960-9822\(97\)70091-5](https://doi.org/10.1016/s0960-9822(97)70091-5).
50. Frost JA, Steen H, Shapiro P, Lewis T, Ahn N, Shaw PE, Cobb MH. 1997. Cross-cascade activation of ERKs and ternary complex factors by Rho family proteins. *EMBO J* 16:6426–6438. <https://doi.org/10.1093/emboj/16.21.6426>.
51. Tang Y, Chen Z, Ambrose D, Liu J, Gibbs JB, Chernoff J, Field J. 1997. Kinase-deficient Pak1 mutants inhibit Ras transformation of Rat-1 fibroblasts. *Mol Cell Biol* 17:4454–4464. <https://doi.org/10.1128/MCB.17.8.4454>.
52. Frost JA, Xu S, Hutchison MR, Marcus S, Cobb MH. 1996. Actions of Rho family small G proteins and p21-activated protein kinases on mitogen-activated protein kinase family members. *Mol Cell Biol* 16:3707–3713. <https://doi.org/10.1128/MCB.16.7.3707>.
53. Thillai K, Lam H, Sarker D, Wells CM. 2017. Deciphering the link between PI3K and PAK: an opportunity to target key pathways in pancreatic cancer? *Oncotarget* 8:14173–14191. <https://doi.org/10.18632/oncotarget.13309>.
54. Liu J-J. 2017. Regulation of dynein-dynactin-driven vesicular transport. *Traffic* 18:336–347. <https://doi.org/10.1111/tra.12475>.
55. Höök P, Vallee RB. 2006. The dynein family at a glance. *J Cell Sci* 119:4369–4371. <https://doi.org/10.1242/jcs.03176>.
56. Pfister KK, Shah PR, Hummerich H, Russ A, Cotton J, Annuar AA, King SM, Fisher EMC. 2006. Genetic analysis of the cytoplasmic dynein subunit families. *PLoS Genet* 2:e1. <https://doi.org/10.1371/journal.pgen.0020001>.
57. Pfister KK, Fisher EMC, Gibbons IR, Hays TS, Holzbaur ELF, McIntosh JR, Porter ME, Schroer TA, Vaughan KT, Witman GB, King SM, Vallee RB. 2005. Cytoplasmic dynein nomenclature. *J Cell Biol* 171:411–413. <https://doi.org/10.1083/jcb.200508078>.
58. Nyarko A, Barbar E. 2011. Light chain-dependent self-association of dynein intermediate chain. *J Biol Chem* 286:1556–1566. <https://doi.org/10.1074/jbc.M110.171686>.
59. Kardon J, Vale R. 2009. Regulators of the cytoplasmic dynein motor. *Nat Rev Mol Cell Biol* 10:854–865. <https://doi.org/10.1038/nrm2804>.
60. Chowdhury S, Ketcham S, Schroer T, Lander G. 2015. Structural organization of the dynein-dynactin complex bound to microtubules. *Nat Struct Mol Biol* 22:345–347. <https://doi.org/10.1038/nsmb.2996>.
61. Olenick M, Holzbaur E. 2019. Dynein activators and adaptors at a glance. *J Cell Sci* 132:jcs227132. <https://doi.org/10.1242/jcs.227132>.
62. Musarrat F. 2019. Cellular and viral determinants of HSV-1 entry and transport. Ph.D. dissertation. Louisiana State University, Baton Rouge, LA.
63. Abramoff M, Magalhaes P, Ram S. 2004. Image processing with ImageJ. *Biophotonics Int* 11:36–42.
64. del Rio T, Ch'ng TH, Flood EA, Gross SP, Enquist LW. 2005. Heterogeneity of a fluorescent tegument component in single pseudorabies virus virions and enveloped axonal assemblies. *J Virol* 79:3903–3919. <https://doi.org/10.1128/JVI.79.7.3903-3919.2005>.

